Title: Cytotoxic effects of nickel nanowires in human fibroblasts

Author: Laura P. Felix Jose E. Perez Maria F. Contreras Timothy Ravasi J*ü*rgen Kosel

PII: S2214-7500(16)30024-5
DOI: http://dx.doi.org/doi:10.1016/j.toxrep.2016.03.004
Reference: TOXREP 345

To appear in:

Received date: 21-11-2015
Revised date: 3-3-2016
Accepted date: 3-3-2016

Please cite this article as: Laura P.Felix, Jose E.Perez, Maria F.Contreras, Timothy Ravasi, J*ddotu*rgen Kosel, Cytotoxic effects of nickel nanowires in human fibroblasts, Toxicology Reports http://dx.doi.org/10.1016/j.toxrep.2016.03.004

Cytotoxic effects of nickel nanowires in human fibroblasts

Laura P. Felix[*, †], Jose E. Perez[*, †], Maria F. Contreras[*], Timothy Ravasi[*, †] and Jürgen Kosel[†]

[*]Division of Biological and Environmental Sciences and Engineering

[†]Division of Computer, Electrical and Mathematical Sciences and Engineering

King Abdullah University of Science and Technology, Thuwal 23955, Kingdom of Saudi Arabia

laura.felixservin@kaust.edu.sa

Jose.Perez@kaust.edu.sa

Maria.Contreras@kaust.edu.sa

timothy.ravasi@kaust.edu.sa

jurgen.kosel@kaust.edu.sa

[†]To whom correspondence should be addressed:

Professor Jürgen Kosel

Telephone: +966 (01) 2808-4360

Email: jurgen.kosel@kaust.edu.sa

Abstract: The increasing interest in the use of magnetic nanostructures for biomedical applications necessitates rigorous studies to be carried out in order to determine their potential toxicity. This work attempts to elucidate the cytotoxic effects of nickel nanowires (NWs) in human fibroblasts WI-38 by a colorimetric assay (MTT) under two different parameters: NW concentration and exposure time. This was complemented with TEM and confocal images to assess the NWs internalization and to identify any changes in the cell morphology. Ni NWs were fabricated by electrodeposition using porous alumina templates. Energy dispersive X-Ray analysis, scanning electron microscopy and transmission electron microscopy imaging were used for NW characterization. The results showed decreased cell metabolic activity for incubation times longer than 24 hours and no negative effects for exposure times shorter than that. The cytotoxicity effects for human fibroblasts were then compared with those reported for HCT 116 cells, and the findings point out that it is relevant to consider the cellular size. In addition, the present study compares the toxic effects of equivalent amounts of nickel in the form of its salt to those of NWs and shows that the NWs are more toxic than the salts. Internalized NWs were found in vesicles inside of the cells where their presence induced inflammation of the endoplasmic reticulum.

***Key Words*:** cytotoxicity; nanotechnology; nanowires; magnetic; human fibroblasts.

1. Introduction

Advancements in fabrication and characterization techniques, as well as the development of new functionalization methods, have increased the interest in nanostructures to provide treatments for certain diseases, to improve our understanding of molecular biology and as tools for a wide range of medical applications. Nanoparticles (NPs) of spherical shape have been the most widely studied nanostructures for their use in drug delivery (Giouroudi and Kosel, 2010; Zhang *et al.*, 2008), diagnostic tools (Gooneratne *et al.*, 2011; Li and Kosel, 2014; Yassine *et al.*, 2014) or as contrast agents in medical imaging (Wang and Wang, 2014). Cylindrical nanostructures such as NWs have been shown to provide improved performance for some biomedical applications. By adjusting the radius and the length, high aspect ratios are achievable. The composition along the wire can be precisely modulated to have multiple domains with different properties (Varadan *et al.*, 2008), allowing single or multiple functionalization using ligands. In addition, magnetic NWs have higher magnetic moment per unit of volume than NPs, allowing them to exert large forces and torques (Hultgren *et al.*, 2003; Song *et al.*, 2010). This last statement has been supported by two comprehensive studies that compared the performance of nickel (Ni) NWs and NPs for cell separation, with the results showing improved performance of NWs over NPs (Gao *et al.*, 2010; Hultgren *et al.*, 2005). Additionally, the saturation magnetization of NWs is over an order of magnitude higher than that of NPs (Gao, *et al.*, 2010; George *et al.*, 2009).

Recent studies have elucidated the potential application of silicon NWs and polycaprolactone NW surfaces in tissue engineering and bone regeneration by showing their capability to support adhesion and proliferation of cells with elongated morphologies (Kuo *et al.*, 2012; Trujillo and Popat, 2014). Other studies (Felton and Reich, 2007) have demonstrated the advantages of NWs in magnetic biosensing, where biomolecules of interest are labeled for their detection and identification. By using NWs, detection can be achieved in the absence of an external magnetic field due to the large remanent magnetization. Moreover, Ni NWs can be internalized by cells such as immortalized fibroblasts (Song, *et al.*, 2010), HeLa and human colorectal carcinoma cells (HCT116) (Margineanu *et al.*, 2016), rat marrow stroma cells, osteoblast cells (MC3T3-E1) and osteosarcoma cells (UMR-106) (Prina-Mello *et al.*, 2006); a capability that can be exploited for diverse disease treatments such as cancer therapy (Contreras *et al.*, 2015).

Cytotoxicity studies of NWs have shown a dependence on factors like material and size. A high concentration of NWs might produce very low toxicity and good biocompatibility in some cell lines such as HeLa cells (Song, *et al.*, 2010), 3T3 fibroblasts (CRL-1658) (Fung *et al.*, 2008) and L929 mouse fibroblast (Johansson *et al.*, 2010), while

being highly toxic for other cell lines including mesenchymal stem cells (Song *et al.*, 2013) and human colorectal carcinoma cells (HCT 116) (Perez *et al.*, 2015). These results together with other contributions have made Ni NWs very interesting for biomedical applications.

Information about the adverse effects of nanostructures on cells and tissues would enable the systematic design of suitable nanostructures for biomedical applications. Cytotoxicity studies provide vital information about the cellular mechanisms involved in nanostructure internalization and toxicity. NWs interact with the cell membrane, triggering their internalization mainly through endocytosis by enclosing them in membrane vesicles (e.g., late endosomes or lysosomes) to be degraded, recycled back to the extracellular environment, transported across cells, or to reach other organelles such as mitochondria (Durán *et al.*, 2014; Verma and Stellacci, 2009). According to some studies, the endocytosis effectiveness can be influenced by the length of the nanostructures, resulting in the activation of membrane receptors specific for a cellular uptake pathway (Kasprzak *et al.*, 2003; Khlebtsov and Dykman, 2011). Smaller nanostructures are internalized more efficiently than longer ones with similar surface characteristics (Thurn *et al.*, 2007). Additionally, the surface charge seems to influence the amount of nanostructures taken up by cells. Non-phagocytic cells have shown a preference for cationic NPs while phagocytic cells take up more efficiently anionic NPs (Alexis *et al.*, 2008; Dowding *et al.*, 2013). The toxic effects of nanostructures inside cells can be driven by their physicochemical properties, such as retention time inside the cell, surface properties, and toxic metabolites. The adverse effects include morphological and structural changes, genotoxicity, and biochemical alterations that trigger different cellular responses such as cell-cycle and proliferation irregularities, diminution of mitochondrial function, activation of cell signaling pathways and cell death (Durán, *et al.*, 2014). It has been revealed that cells are able to break up iron NWs aggregates into smaller ones that were later degraded (Safi *et al.*, 2011); the NWs and the remains of the degradation were found either in vesicular compartments or directly dispersed in the cytosol. The resulting ionic forms due to NW degradation are able to interact with and alter the intracellular environment (Fung, *et al.*, 2008).

A review article about Ni carcinogenesis (Kasprzak, *et al.*, 2003) concluded that Ni^{2+} ions released from NPs reached the nucleus in greater amounts than Ni^{2+} ions from water-soluble Ni(II) sulfate, resulting in a higher cytotoxicity. According to the authors, this was due to the relatively inefficient uptake mechanisms of water-soluble Ni (II) compounds (i.e. diffusion, iron/calcium channels). Some other studies have shown that the toxicity of a material in a certain form (e.g. NW) cannot be inferred from the toxicity of the same material in a different shape

(e.g. NP) (Song, *et al.*, 2010). A good example is asbestos, a "benign" silicate that is highly toxic in its fibrous form (Song, *et al.*, 2010). Therefore, cytotoxicity studies must be carried out for specific materials in specific geometries and for specific cell lines.

This work aims to study the viability of human fibroblasts when grown in the presence of Ni NWs at different concentrations and for incubation times of 24, 48 and 72 hours. The results are compared to those obtained for Ni salt to get further insight into the cytotoxic mechanisms. In addition, the NW internalization assessment is approached using TEM and confocal images that as well elucidate any changes in the fibroblasts. To our knowledge, this is the first systematic cytotoxicity study done in human fibroblasts WI-38 using ferromagnetic NWs, where the toxic effects of equivalent amounts of Ni in its ionic form and in its NW form are compared.

2. Materials and methods

2.1 Fabrication and characterization of Ni NWs

Ni NWs were fabricated by electrodeposition in highly ordered porous aluminum oxide (PAO) templates. High purity Aluminum (Al) disks (99.999% purity, Goodfellow) of 2.5 cm in diameter and 0.5 mm in thickness were subjected to cleaning and electropolishing to remove contaminants from the substrate surface. After that, a two-step anodization process using 0.3 M oxalic acid was used to obtain a highly ordered PAO template. The first anodization was carried out by applying a constant voltage of 40 V to the Al disk for 24 hours, maintaining the temperature within 2-4°C and keeping the solution under constant stirring (~200 rpm). The result was an aluminum oxide (alumina) layer on the Al surface with disordered pores and ordered domains on the Al substrate. The alumina layer was chemically removed by using a chromium-based solution consisting of 0.2 M CrO_3 and 0.4 M H_3PO_4 in DI water at 30°C for 12 hours. The second anodization was carried out using the same setup and under the same conditions of the first anodization process, with the exception of the anodization time being 20 hours. The result was a membrane with highly ordered nanopores and a narrow diameter distribution. To prepare the sample for the electrodeposition process, the aluminum on the backside of the Al disk was removed using a copper solution 1.67% (w/v) of $CuCl_2 \cdot 2H_2O$ and 49.16% (v/v) of HCl. Afterwards, the pores were opened using 5% (v/v) phosphoric acid solution and a gold layer (~200 nm) was sputtered on the backside of the membrane. These three steps were done in order to establish a good electrical contact between the pore and the base of the substrate. Finally, the pores were filled with Ni by direct current electrodeposition using a Ni solution consisting of 46 g/L of Ni (II) chloride

hexahydrate ($NiCl_2 \cdot 6H_2O$), 40 g/L of boric acid (H_3BO_4) and 300 g/L of Ni (II) sulfate hexahydrate ($NiSO_4 \cdot 6H_2O$). For the electrodeposition process, a reference voltage of -1 V (vs. Ag/AgCl) was used and the time was adjusted to obtain Ni NWs of 1 μm in length. After electrodeposition, the gold layer on the backside of the sample was removed using reactive ion etching. The template pieces were then put in an Eppendorf tube containing 1 ml of 1 M sodium hydroxide (NaOH) solution and left for 24 hours to selectively dissolve the alumina. The NaOH solution was replaced with 1 ml of chrome solution and left for 24 hours in a Thermomixer® comfort (Eppendorf) at 40°C and 300 rpm. The Eppendorf tube was put in a magnetic holder (Dynamag^{TM}-2) to collect the NWs, and then the chrome solution was discarded and replaced with ethanol. The NWs were suspended and shaken for cleaning and disposal of traces of NaOH, chromium-based solution and aluminum membrane. This step was repeated several times to ensure complete removal of the chromium-based solution.

Energy dispersive X-Ray analysis (EDX) was used to obtain the elemental composition of the Ni NWs. Scanning electron microscopy (SEM) was used to visualize the filled pores, the alumina template and released Ni NWs. Transmission electron microscopy (TEM) was used to characterize their morphology and to study the oxide layer formed on their surface. To estimate the number of NWs corresponding to each sample, the number of pores was calculated for a defined area of the alumina template from SEM images using ImageJ software. This value was multiplied by the total area and divided by the area of the alumina template from the SEM image.

2.2 Cell culture

Human fibroblasts WI-38 (ATCC® CCL-75™) cells were cultured in Eagle's minimum essential medium (EMEM Quality Biological Inc.) supplemented with Sodium Pyruvate (Gibco®), non-essential aminoacids solution (MEM NEAA Gibco®), 10% fetal bovine serum (FBS) and 1% penicillin/streptomycin. The cells were incubated at 37 °C in a humidified incubator with 5% carbon dioxide (CO_2). Each time the cell culture reached a confluence of 70-80%, the cells were washed twice with Dulbecco's phosphate-buffered saline (DPBS) calcium and magnesium free and detached with 0.05% trypsin. Trypan blue staining and a hemocytometer were used for cell counting.

2.3 Cytotoxicity assay

The 3-(4, 5-dimethylthiazol-2yl)-2, 5-diphenyl tetrazolium bromide (MTT) cell proliferation assay (Vibrant®) was chosen as the method to determine and evaluate NW cytotoxicity in terms of cell metabolic activity.

In a clear, flat-bottom 96-well plate (Fisher Scientific), cells suspended in 100 µl of EMEM medium were seeded in triplicates for each condition tested, as well as a negative control (cells without NWs). This setup was performed three times; one 96-well plate per exposure time (24, 48 and 72 hours) and a full experiment consisted of three independent biological replicas. All plates were placed in the incubator for 24 hours to achieve proper attachment and cell density. After that time, the cells were treated with either NWs or Ni salts (Ni (II) sulfate hexahydrate and Ni (II) chloride hexahydrate). For the Ni salts experiments, the concentration of Ni in µg/ml was calculated to be equivalent to each of the NW concentration used for Ni NWs experiments by:

$$Total\ mass = m \cdot (no.of\ NWs) \cdot (no.of\ cells) \cdot (no.of\ wells)\ . \quad (2)$$

Where *m* is the mass of a single NW. The desired concentrations of NWs or Ni salts were diluted in EMEM medium and added to each well. For the negative control wells medium alone was added. All plates were placed in the incubator. After the desired incubation time, the media was carefully discarded from all wells and the cells were washed twice with PBS. Then, 100 □l of 10% v/v MTT solution (5 mg/ml in PBS) in medium was added. After 3 hours of incubation, the MTT solution was discarded and replaced by 100 □l of 20% (w/v) sodium dodecyl sulfate solution and 0.6% (v/v) 37% HCl in dimethyl sulfoxide, which acted as a cell lysis buffer, breaking the cells and allowing the purple crystals to be released in the solution. The 96 well plates were then shaken in a Multi-Microplate Genie (Scientific Industries) to dissolve the MTT crystals, resulting in a homogeneous color of the solution. The concentration of purple crystals was determined by optical density (OD) measurements using an xMark™ microplate absorbance spectrophotometer (Bio-Rad). A 570 nm wavelength and a reference wavelength of 630 nm were used. Each OD value was subtracted from the reference wavelength to eliminate the background signal. Cell viability at each condition was determined using equation (3):

$$Cell\ viability(\%) = \frac{OD_{570-630}[Condition]}{OD_{570-630}[Negative\ control]} * 100\%\ . \quad (3)$$

The data points were presented as a percentage of control cells and each one is an average of the respective triplicates.

The Ni salt solution was prepared with $NiSO_4 \cdot 6H_2O$ and $NiCl_2 \cdot 6H_2O$ and later diluted in EMEM medium. These were the same salts used to prepare the Ni solution for electrodeposition during NW fabrication. The concentration

of Ni in in the solution (μg/ml) was equivalent to the amount of Ni in the NW experiments. The equivalent amount was found by calculating the mass of a single NW using Equation (1), which was 2.5×10^{-9} μg.

2.4 Confocal Microscopy

The cells were seeded in a Lab-Tek™ II Chambered cover glass and incubated 24 hours, reaching a confluence of ~80%. Later, Ni NWs where added to the cells at a concentration of 22.5 μg/mL and the plates were placed in the incubator for 24, 48 and 72 hours. After each time, the cells were washed with PBS and fixed with 3.7 % (v/v) formaldehyde diluted in PBS, which was removed after 5 minutes of incubation at room temperature. The cells were washed twice with PBS and then the nuclei of the cells were stained with a 300 nM solution of 4',6-diamidino-2-phenylindole (DAPI) stain. The solution was removed after 8 minutes of incubation at room temperature and the cells were washed three times with PBS. Fluorescence was observed using a Zeiss LSM 710 Inverted Confocal Microscope with an excitation and emission wavelength of 360 nm and 460 nm, respectively.

2.5 TEM internalization studies

Human fibroblasts cells were seeded in 6-well plates and incubated for 24 hours. After that the cells were treated with Ni NWs at a concentration of 22.5 μg/mL and incubated for 24, 48 and 72 hours. After each exposure time, the medium was discarded and the cells were fixed with 2.5% [v/v] glutaraldehyde in cacodylate buffer (0.1 M, pH 7.4). Fixed cells were treated with reduced osmium (1:1 mixture of 2% aqueous potassium ferrocyanide) as described previously (Karnovsky, 1971), dehydrated in ethanol and embedded in Epoxy resin.

Sections of 100-150 nm thickness were collected on copper grids and stained with lead citrate. Finally, imaging was performed using a transmission electron microscope operating at 300 kV (Titan Cryo Twin, FEI Company, Hillsboro, OR). Images were recorded by a 4k×4k CCD camera (Gatan Inc., Pleasanton, CA).

2.6 Statistical Analysis

Results are presented as mean ± standard deviation (SD). The statistical significance was determined by one-way analysis of variance (ANOVA) using MATLAB software. Differences were considered significant for $p<0.05$.

3. Results

3.1 Elemental and morphological characterization of Ni NWs

Fig. 1A shows the EDX spectrum of the NWs. The copper peak is the result of using a copper grid to mount the sample. The small peak of oxygen can be attributed to the ethanol used to wash the NWs. Figure 1B shows a close view of a single Ni NW that reveals the presence of an oxide layer with a thickness of ~3.1 nm, possibly as a result of the release process or the NWs exposition to air.

SEM images were taken to determine the diameter (Fig. 2A) and length (Fig. 2B) distribution using ImageJ software. In both cases, a representative sample of 20 NWs and pores was used. On average, the NWs diameter and length were found to be 31 nm and 1 μm, respectively (Fig. 2C), resulting in an aspect ratio of about 32.

3.2 Cytotoxicity Effects of Ni NWs

The MTT assay is a colorimetric assay based on the principle that metabolically active cells are able to reduce the MTT tetrazolium salt, a yellow water-soluble salt, to formazan, an aqueous purple insoluble product. The reduction process is carried out mainly at the mitochondrial level (Dobrucki, 2001) by mitochondrial succinate dehydrogenase. The formazan is solubilized and then the concentration is determined by the OD value, which is used as an indicator of cell viability.

Before conducting the cell viability experiments, it was confirmed that the Ni NWs did not interfere with the MTT assays. To this end, Ni NWs were suspended in 100 □l of EMEM medium and a control consisting of 100 □l of EMEM medium was added to 96-well plate in triplicates. Three exposure times were tested (24, 48 and 72 hour), showing that the OD values were the same for the sample with NWs and for the control (data not shown).

The first cytotoxicity assay was done to evaluate the effects of Ni NWs as a function of NW concentration and incubation time. The results (Fig. 3A) showed high cell viability (>80%) when the concentration was 0.22 μg/mL or 2.25 μg/mL, for any time point. For the 22.5 μg/mL concentration, the cell viability was high (96%) after 24 hours, but further this value decreased up to 75% and 72% after 48 or 72 hours, respectively. Overall, cell viability at the mitochondrial level decreased while NW concentration and incubation time increased.

One of the challenges of evaluating cytotoxicity after long incubation periods (i.e. 72 hours) is cell overconfluence, which might lead to a decrease of the cells' metabolic activity. The obtained OD values of untreated cells at different incubation times did not show significant variations for all the MTT experiments. In contrast, OD values showed significant variations when the NW concentration was modified. These results confirmed that confluence at different incubation times did not significantly affect cell metabolic activity, and any loss of cell viability was caused by the presence of Ni NWs.

Cytotoxicity studies were done on colon cancer cells (HCT 116) exposed to 1 μm long Ni NWs at different concentrations (10:1, 50:1, 100:1, 200:1 and 1000:1 NWs per cell) and the results showed high cell viability (>80%) up to the 100:1 concentration and 48 hours of incubation. For the rest, cell viability was decreasing up to 40%, depending on concentration and time (Perez *et al.*, 2014). Comparing those results with the ones obtained for WI-38 cells (Fig. 3A) in this work, it can be concluded that HCT 116 cells showed lower viability than WI-38 in the presence of Ni NWs. This might be explained by the difference in cell size (fibroblasts 4831.7 μm^2 and colon cancer cells ~804.3 μm^2 area); meaning that even though the proportion between NW concentration and estimated number of cells at the time of the treatment are the same for both cell lines, the NW concentration per cell volume is less in the case of fibroblasts. The last statement refers to the fact that the number of WI-38 cells was around five times less than the number of HCT 116 at the time of the treatment with NWs. To confirm this idea, a second MTT assay using WI-38 cells exposed to a higher NW concentration was carried out. The experiment was performed using Ni NWs at concentrations of 1.18 μg/mL, 11.88 μg/mL and 118.8 μg/mL, which correspond to those used on HCT 116 cells.

As shown in Fig. 3B, the cells remained more than 80% viable up to the 11.18 □g/mL concentration and 48 hours of incubation. The cell viability decreased up to 74% at 11.88 μg/mL concentration, after 72 hours. Further increasing the concentration to 118.8 μg/mL, led to abrupt decreases in cell viability: ~70%, ~56% and ~47% after 24, 48 and 72 hours, respectively. These values are within the same range as those reported for HCT 116 cells, confirming the reasoning above that not just the concentration of NWs and incubation time are relevant, but that the cellular size and volume play an indirect role in the NWs metabolism and therefore in their cytotoxicity.

3.3 Cytotoxicity Effects of Ni salts

In order to elucidate whether the side products of Ni NWs degradation are the reason for or contribute to their toxicity, MTT assays were performed using Ni salts dissolved in EMEM medium. The cell viability for Ni salts with a concentration equivalent to the amount of Ni NWs, after 24 and 48 hours was above 90% and approximately 88%

after 72 hours (Fig. 3C). Surprisingly, the results showed no significant difference between the treated cells and their respective controls, with exception of the mean value for 2.25 μg/mL concentration after 72 hours. Overall, the cell viability seems to be independent of the Ni salts concentration and exposure time.

These results show that Ni NWs are more toxic than the Ni salts. A possible explanation for the higher cytotoxicity of the NWs can be attributed to a different cytotoxicity mechanism tied to their morphology (cylindrical shape).

3.4 Internalization of Ni NWs

Fluorescence images of cells with DAPI stained nucleus were taken using confocal microscopy. As shown in the images (Fig. 3D, 3E and 3F), the NWs are interacting with the cells; however, the nuclei's morphology seems to be unaffected.

In order to assess internalization of Ni NWs by WI-38 cells, TEM images were taken at different exposure times (Fig. 4). After 24 hours, NWs were already found inside the cells. They were mainly observed as dark dense aggregates inside cellular vesicles, possibly lysosomes. Some of the images (Fig.4, 24 hours) showed notorious alteration of the normal size of the endoplasmic reticulum (ER) when compared to the untreated cells. A closer view on the TEM images confirms that the Ni NWs are typically agglomerated in a random shape (Fig. 5).

4. Discussion

The results show that human fibroblasts are capable of internalizing and encapsulating Ni NWs in vesicles. The internalized Ni NWs do not seem to affect the cell viability of the human fibroblasts during the first 24 hours. However, their toxic effects become notorious for longer exposure times and at higher concentrations. These results are in agreement with previous studies of Fe NWs in HeLa cells (Song, *et al.*, 2010); Ni NWs in colon cancer cells (HCT 116) (Perez, *et al.*, 2014) and monocytic cells (THP-1) (Byrne *et al.*, 2009); gold NPs in human fetal lung (MRC-5) (Jasmine J. Li, 2008) and primary human dermal fibroblasts (CF-31) (Mironava *et al.*, 2010).

In general, the cell viability behavior is similar among different cell lines regardless of the nanostructure materials (higher concentrations and longer exposure times result in more severe toxic effects); however, different cell lines show different cell viability for the same conditions. The cytotoxic effects of Ni NWs on human fibroblasts (WI-38) reported in the present study differ from those reported in the past for Ni NWs on colon cancer cells (Perez, *et al.*, 2014).

Moreover, the data shows that Ni salts are less toxic than Ni NWs. The higher cytotoxicity of the NWs suggests that the shape plays an important role. Previous studies reported a similar conclusion when comparing the toxic effects of Ni NPs with those for soluble Ni at equivalent concentrations (Cristina Ispas, 2009) and Ag NPs with its ionic form (Sambale *et al.*, 2015).

Previous studies reported that Ni NWs are stable in different biological solutions (Raphael *et al.*, 2010), with a passivation oxide layer forming around the NW core. Therefore, the amount of NW material that gets dissolved in cell culture medium is minimal. Once internalized, the cells try to break down the NWs. The thin oxide layer formed around the Ni core gets easily dissolved inside the cells, resulting in the release of Ni^{2+} and further oxidation of the Ni core (Perez, *et al.*, 2015). This elucidates the important role that the oxide and Ni^{2+} play in the cytotoxic effect of the Ni NWs, as supported by previous studies (ChangGuo Ma, 2014; Kasprzak, *et al.*, 2003; Perez, *et al.*, 2015).

TEM images show changes in the size of the ER, suggesting that Ni NWs might cause ER stress under certain conditions. An indication of ER stress is the accumulation of unfolded proteins in the ER that overload it, resulting in ER swelling (Chen *et al.*, 2014; Eun-Jung Park, 2014; Jean-Christophe Simard, 2015). ER stress has previously been identified as a cellular response to the cytotoxicity of Ni NWs (Zhang *et al.*, 2012). The data presented in this study shows ER swelling only after 24 hours of exposure.

5. Conclusions

This study showed the cytotoxicity of Ni NWs on WI-38 cells (human fibroblasts) by measuring cell viability at different incubation times and NW concentrations. Significant toxic effects were found for NWs mostly after 48 hours at high concentrations with cell viability decreasing as incubation time increased, results that confirmed previous findings with Fe and gold NWs, as well as with NPs. In addition, the comparison of the toxic effects of NWs among different cell lines suggested that the size of the cell and the cell type also play a crucial role in the toxic effects of the NWs, and a normalization of the nanoparticle concentration to the cell size should be considered for such comparisons.

The toxic effects of Ni in the form of its salts were compared with those of Ni NWs. The results showed that the Ni salts are less toxic than Ni NWs, which is similar to previous findings for Ag NPs and ions. The results indicate that there are effects related to the material and effects related to the morphology. It is also important to consider the

thin oxide layer surrounding the Ni core of the NW. This layer gets easily dissolved inside of the cells and acts as a source for Ni^{2+}, contributing to the toxic effects.

TEM images showed that some of the NWs were internalized and encapsulated in vesicles within 24 hours. The presence of NWs inside the cell induced alterations of the size of the endoplasmic reticulum, which could be an ER stress indicator in the cells. Such response has been previously reported but no TEM images of ER alterations had been shown.

Acknowledgements

Research reported in this publication was supported by the King Abdullah University of Science and Technology (KAUST).

References

Alexis, F., Pridgen, E., Molnar, L. K., and Farokhzad, O. C. (2008). Factors affecting the clearance and biodistribution of polymeric nanoparticles. *Mol Pharm* **5**(4), 505-15, 10.1021/mp800051m.

Byrne, F., Prina-Mello, A., Whelan, A., Mohamed, B. M., Davies, A., Gun'ko, Y. K., Coey, J. M. D., and Volkov, Y. (2009). High content analysis of the biocompatibility of nickel nanowires. *Journal of Magnetism and Magnetic Materials* **321**(10), 1341-1345, Doi 10.1016/J.Jmmm.2009.02.035.

ChangGuo Ma, M. S., Ye Zhang, ManQing Yan, Min Zhang, Hong Bi (2014). Nickel nanowires induce cell cycle arrest and apoptosis by generation of reactive oxygen species in HeLa cells. *ELSEVIER* **1**, 114–121.

Chen, R., Huo, L., Shi, X., Bai, R., Zhang, Z., Zhao, Y., Chang, Y., and Chen, C. (2014). Endoplasmic reticulum stress induced by zinc oxide nanoparticles is an earlier biomarker for nanotoxicological evaluation. *ACS Nano* **8**(3), 2562-74, 10.1021/nn406184r.

Contreras, M., Sougrat, R., Zaher, A., Ravasi, T., and Kosel, J. (2015). Non-chemotoxic induction of cancer cell death using magnetic nanowires. *International Journal of Nanomedicine* **10** 2141, 10.2147/ijn.s77081.

Cristina Ispas, D. A., Avni Patel, Dan V. Goia, Silvana Andreescu and Kenneth N. Wallace (2009). Toxicity and developmental defects of different sizes and shape nickel nanoparticles in zebrafish. *Environmental Science & Technology* **43**(16), 6349–6356.

Dobrucki, T. B. a. J. (2001). Mitochondrial and Nonmitochondrial Reduction of MTT: Interaction of MTT With TMRE, JC-1, and NAO Mitochondrial Fluorescent Probes. *Cytometry* **47**, 236-242.

Dowding, J. M., Das, S., Kumar, A., Dosani, T., McCormack, R., Gupta, A., Sayle, T. X. T., Sayle, D. C., Kalm, L. v., Seal, S., and Self, W. T. (2013). Cellular Interaction and Toxicity Depend on Physicochemical Properties and Surface Modification of Redox-Active Nanomaterials. *Acs Nano* **7**(6), 4855–4868, Doi 10.1021/Nn305872d.

Durán, N., Guterres, S. S., Alves, O. L., and Zucolotto, V. (2014). In Vitro Cytotoxicity Assays of Nanoparticles on Different Cell Lines. In *Nanotoxicology: Materials, Methodologies, and Assessments.* (doi: 10.1007/978-1-4614-8993-1. Springer Science & Businnes Media.

Eun-Jung Park, D.-H. C., Younghun Kim, Eun-Woo Lee, Jaewhan Song, Myung-Haing Cho, Jae-Ho Kim, Sang-Wook Kim (2014). Magnetic iron oxide nanoparticles induce autophagy preceding apoptosis through mitochondrial damage and ER stress in RAW264.7 cells. *Toxicology in Vitro* **28**, 1402-1412.

Felton, E. J., and Reich, D. H. (2007). Biological Applications of Multifunctional Magnetic Nanowires. In *Biomedical Applications of Nanotechnology* (D. L. L.-P. Vinod Labhasetwar, Ed.) Eds.) doi: 10.1002/9780470152928, pp. 272. John Wiley & Sons.

Fung, A. O., Kapadia, V., Pierstorff, E., Ho, D., and Chen, Y. (2008). Induction of cell death by magnetic actuation of nickel nanowires internalized by fibroblasts. *Journal of Physical Chemistry C* **112**(39), 15085-15088, Doi 10.1021/Jp806187r.

Gao, N., Wang, H., and Yang, E. H. (2010). An experimental study on ferromagnetic nickel nanowires functionalized with antibodies for cell separation. *Nanotechnology* **21**(10), 105107, 10.1088/0957-4484/21/10/105107.

George, T., Gao, N., Yang, X., Tsai, Y.-T., Chu, G. M., Wang, H., Yang, E.-H., Islam, M. S., and Dutta, A. K. (2009). Antibody-functionalized magnetic nanowires for cell purification **7318**, 73181E-73181E-6, 10.1117/12.818402.

Giouroudi, I., and Kosel, J. (2010). Recent progress in biomedical applications of magnetic nanoparticles. *Recent Pat Nanotechnol* **4**(2), 111-8.

Gooneratne, C. P., Giouroudi, I., Liang, C., and Kosel, J. r. (2011). A giant magnetoresistance ring-sensor based microsystem for magnetic bead manipulation and detection. *Journal of Applied Physics* **109**(7), 07E517, 10.1063/1.3536822.

Hultgren, A., Tanase, M., Chen, C. S., Meyer, G. J., and Reich, D. H. (2003). Cell manipulation using magnetic nanowires. *Journal of Applied Physics* **93**(10), 7554-7556, Doi 10.1063/1.1556204.

Hultgren, A., Tanase, M., Felton, E. J., Bhadriraju, K., Salem, A. K., Chen, C. S., and Reich, D. H. (2005). Optimization of yield in magnetic cell separations using nickel nanowires of different lengths. *Biotechnology Progress* **21**(2), 509-515, Doi 10.1021/Bp049734w.

Jasmine J. Li, L. Z., Deny Hartono, Choon-Nam Ong, Boon-Huat Bay, and Lin-Yue Lanry Yung (2008). Gold Nanoparticles Induce Oxidative Damage in Lung Fibroblasts In Vitro. *Advanced Materials* **20**, 138-142, 10.1002/adma.200701853.

Jean-Christophe Simard, F. V., Rafael de Liz, Valerie Lavastre and Denis Girard (2015). Silver nanoparticles induce degradation of the endoplasmic reticulum stress sensor Activating Transcription Factor-6 leading to activation of the NLRP-3 inflammasome. *The Journal of Biological Chemistry* doi: 10.1074/jbc.M114.610899, 10.1074/jbc.M114.610899.

Johansson, F., Jonsson, M., Alm, K., and Kanje, M. (2010). Cell guidance by magnetic nanowires. *Exp Cell Res* **316**(5), 688-94, 10.1016/j.yexcr.2009.12.016.

Karnovsky, M. (1971). Use of ferrocyanide-reduced osmium tetroxide in electron microscopy. *Proc 11th Annu Meet Am Soc Cell Biol* **51**, 146.

Kasprzak, K. S., Jr., F. W. S., and Salnikow, K. (2003). Nickel carcinogenesis. *Mutation Research/Fundamental and Molecular Mechanisms of Mutagenesis* **533**(1-2), 67–97, 10.1016/j.mrfmmm.2003.08.021.

Khlebtsov, N., and Dykman, L. (2011). Biodistribution and toxicity of engineered gold nanoparticles: a review of in vitro and in vivo studies. *Chem Soc Rev* **40**(3), 1647-71, 10.1039/c0cs00018c.

Kuo, S. W., Lin, H. I., Ho, J. H., Shih, Y. R., Chen, H. F., Yen, T. J., and Lee, O. K. (2012). Regulation of the fate of human mesenchymal stem cells by mechanical and stereo-topographical cues provided by silicon nanowires. *Biomaterials* **33**(20), 5013-22, 10.1016/j.biomaterials.2012.03.080.

Li, F., and Kosel, J. (2014). An efficient biosensor made of an electromagnetic trap and a magneto-resistive sensor. *Biosens Bioelectron* **59**, 145-50, 10.1016/j.bios.2014.03.035.

Margineanu, M. B., Julfakyan, K., Sommer, C., Perez, J. E., Contreras, M. F., Khashab, N., Kosel, J., and Ravasi, T. (2016). Semi-automated quantification of living cells with internalized nanostructures. *J Nanobiotechnology* **14**(1), 4, 10.1186/s12951-015-0153-x.

Mironava, T., Hadjiargyrou, M., Simon, M., Jurukovski, V., and Rafailovich, M. H. (2010). Gold nanoparticles cellular toxicity and recovery: effect of size, concentration and exposure time. *Nanotoxicology* **4**(1), 120-37, 10.3109/17435390903471463.

Perez, J. E., Contreras, M. F., Vilanova, E., Felix, L. P., Margineanu, M. B., Luongo, G., Porter, A. E., Dunlop, I. E., Ravasi, T., and Kosel, J. (2015). Cytotoxicity and intracellular dissolution of nickel nanowires. *Nanotoxicology* doi: 10.3109/17435390.2015.1132343, 1-38, 10.3109/17435390.2015.1132343.

Perez, J. E., Contreras, M. F., Vilanova, E., Ravasi, T., and Kosel, J. (2014). Cytotoxicity and Effects on Cell Viability of Nickel Nanowires. In *2013 International Conference on Biological, Medical and Chemical Engineering (BMCE2013)* (doi, pp. 178. DEStech Publications, Inc.

Prina-Mello, A., Diao, Z., and Coey, J. M. (2006). Internalization of ferromagnetic nanowires by different living cells. *J Nanobiotechnology* **4**, 9, 10.1186/1477-3155-4-9.

Raphael, M. P., Christodoulides, J. A., Qadri, S. N., Simpkins, B. S., and Byers, J. M. (2010). Magnetic moment degradation of nanowires in biological media: real-time monitoring with SQUID magnetometry. *Nanotechnology* **21**(28), 285101, 10.1088/0957-4484/21/28/285101.

Safi, M., Yan, M. H., Guedeau-Boudeville, M. A., Conjeaud, H., Garnier-Thibaud, V., Boggetto, N., Baeza-Squiban, A., Niedergang, F., Averbeck, D., and Berret, J. F. (2011). Interactions between Magnetic Nanowires and Living Cells: Uptake, Toxicity, and Degradation. *Acs Nano* **5**(7), 5354-5364, Doi 10.1021/Nn201121e.

Sambale, F., Wagner, S., Stahl, F., Khaydarov, R. R., Scheper, T., and Bahnemann, D. (2015). Investigations of the Toxic Effect of Silver Nanoparticles on Mammalian Cell Lines. *Journal of Nanomaterials* **2015**, 1-9, 10.1155/2015/136765.

Song, M. M., Song, W. J., Bi, H., Wang, J., Wu, W. L., Sun, J., and Yu, M. (2010). Cytotoxicity and cellular uptake of iron nanowires. *Biomaterials* **31**(7), 1509-17, 10.1016/j.biomaterials.2009.11.034.

Song, Y. H., Ju, Y., Zhang, L., Morita, Y., and Song, G. B. (2013). Fabrication of Cu Nanowires and Its Effect on Proliferation of Mesenchymal Stem Cells. *Advanced Materials Science and Technology, (Ifamst-8)* **750**, 56-59, Doi 10.4028/http://Www.Scientific.Net/Msf.750.56.

Thurn, K. T., Brown, E., Wu, A., Vogt, S., Lai, B., Maser, J., Paunesku, T., and Woloschak, G. E. (2007). Nanoparticles for applications in cellular imaging. *Nanoscale Res Lett* **2**(9), 430-41, 10.1007/s11671-007-9081-5.

Trujillo, N. A., and Popat, K. C. (2014). Increased Adipogenic and Decreased Chondrogenic Differentiation of Adipose Derived Stem Cells on Nanowire Surfaces. *Materials* **7**, 2605-2630.

Varadan, V. K., Chen, L., and Xie, J. (2008). Magnetic Nanowires and their Biomedical Applications. In *Nanomedicine: Design and Applications of Magnetic Nanomaterials, Nanosensors and Nanosystems.* (J. W. Sons, Ed.) Eds.) doi: 1 ed., pp. 215-272.

Verma, A., and Stellacci, F. (2009). Effect of Surface Properties on Nanoparticle–Cell Interactions. *Small* doi, 1-10.

Verma, N. K., Conroy, J., Lyons, P. E., Coleman, J., O'Sullivan, M. P., Kornfeld, H., Kelleher, D., and Volkov, Y. (2012). Autophagy induction by silver nanowires: a new aspect in the biocompatibility assessment of nanocomposite thin films. *Toxicol Appl Pharmacol* **264**(3), 451-61, 10.1016/j.taap.2012.08.023.

Wang, E. C., and Wang, A. Z. (2014). Nanoparticles and their applications in cell and molecular biology. *Integr Biol (Camb)* **6**(1), 9-26, 10.1039/c3ib40165k.

Yassine, O., Gooneratne, C. P., Abu Smara, D., Li, F., Mohammed, H., Merzaban, J., and Kosel, J. (2014). Isolation of cells for selective treatment and analysis using a magnetic microfluidic chip. *Biomicrofluidics* **8**(3), 034114, 10.1063/1.4883855.

Zhang, L., Gu, F. X., Chan, J. M., Wang, A. Z., Langer, R. S., and Farokhzad, O. C. (2008). Nanoparticles in medicine: Therapeutic applications and developments. *Clinical Pharmacology & Therapeutics* **83**(5), 761-769, Doi 10.1038/Sj.Clpt.6100400.

Zhang, R., Piao, M. J., Kim, K. C., Kim, A. D., Choi, J. Y., Choi, J., and Hyun, J. W. (2012). Endoplasmic reticulum stress signaling is involved in silver nanoparticles-induced apoptosis. *Int J Biochem Cell Biol* **44**(1), 224-32, 10.1016/j.biocel.2011.10.019.

FIGURES:

Figure 1. Composition analysis and morphology of Ni NWs. A) EDX spectrum of released Ni NWs. B) TEM image of a single Ni NW.

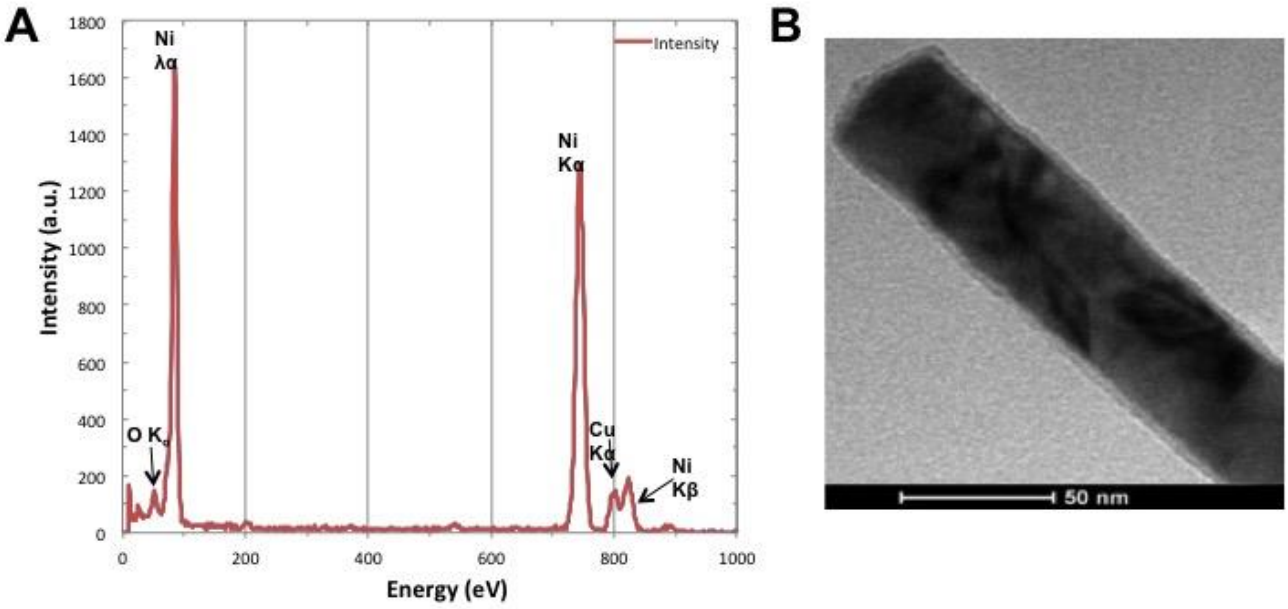

Figure 2. Characterization of Ni NWs. SEM images of A) the filled pores and the alumina template, B) released NWs, C) pore sizes and length distributions for the sample used during this work.

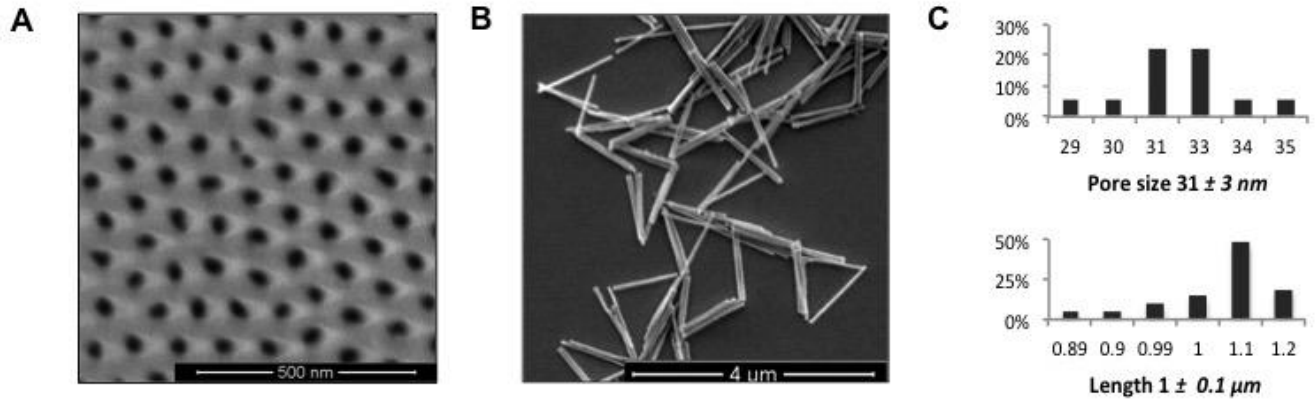

Figure 3. MTT assay of cell viability on WI-38 cells: A) and B) cell viability after treatment with 1 μm Ni NWs assessing different concentrations. C) Cell viability after treatment with Ni salts. NC = negative control. Percent viability of cells was expressed relative to control cells. The data show mean values ± standard deviation, n = 3, *$p < 0.05$, ** $p < 0.01$ from the respective control. Confocal images of fibroblasts D) after 24, E) 48 and F) 72 hours of incubation with 1 μm long Ni NWs with a 22.5 μg/mL concentration. The nuclei (blue) were stained with DAPI. White arrows indicate some of the NWs.

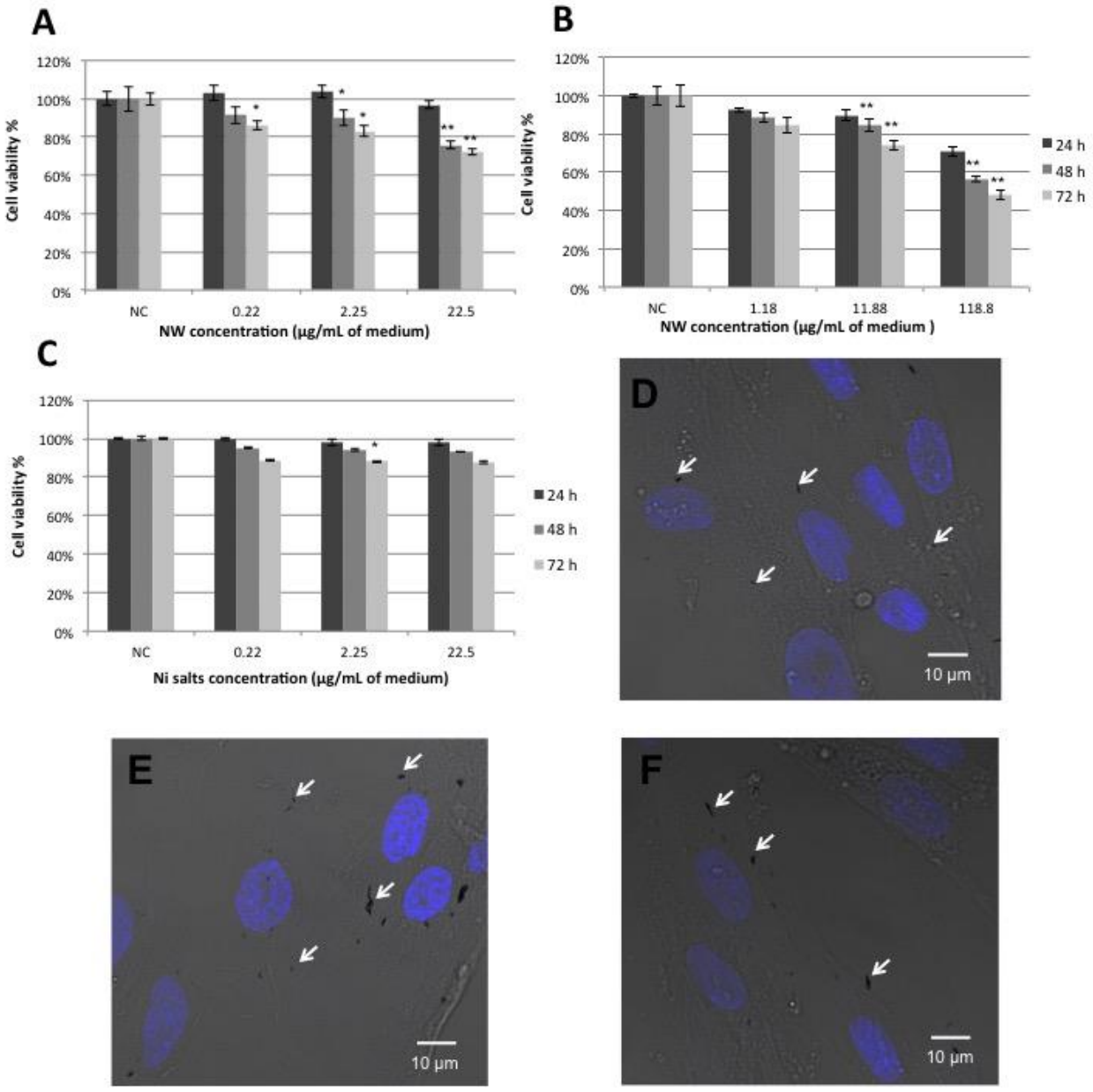

Figure 4. TEM images of WI-38 fibroblasts treated with Ni NWs. Internalized 1 μm long Ni NWs (right column) after (A) 24, (B) 48 and (C) 72 hours. The Ni NWs were found inside vesicles, most likely lysosomes (red arrows). In some of the pictures alteration of the normal size of the endoplasmic reticulum was observed (black narrows). Their respective controls are shown in the left column. Scale bars=1 μm.

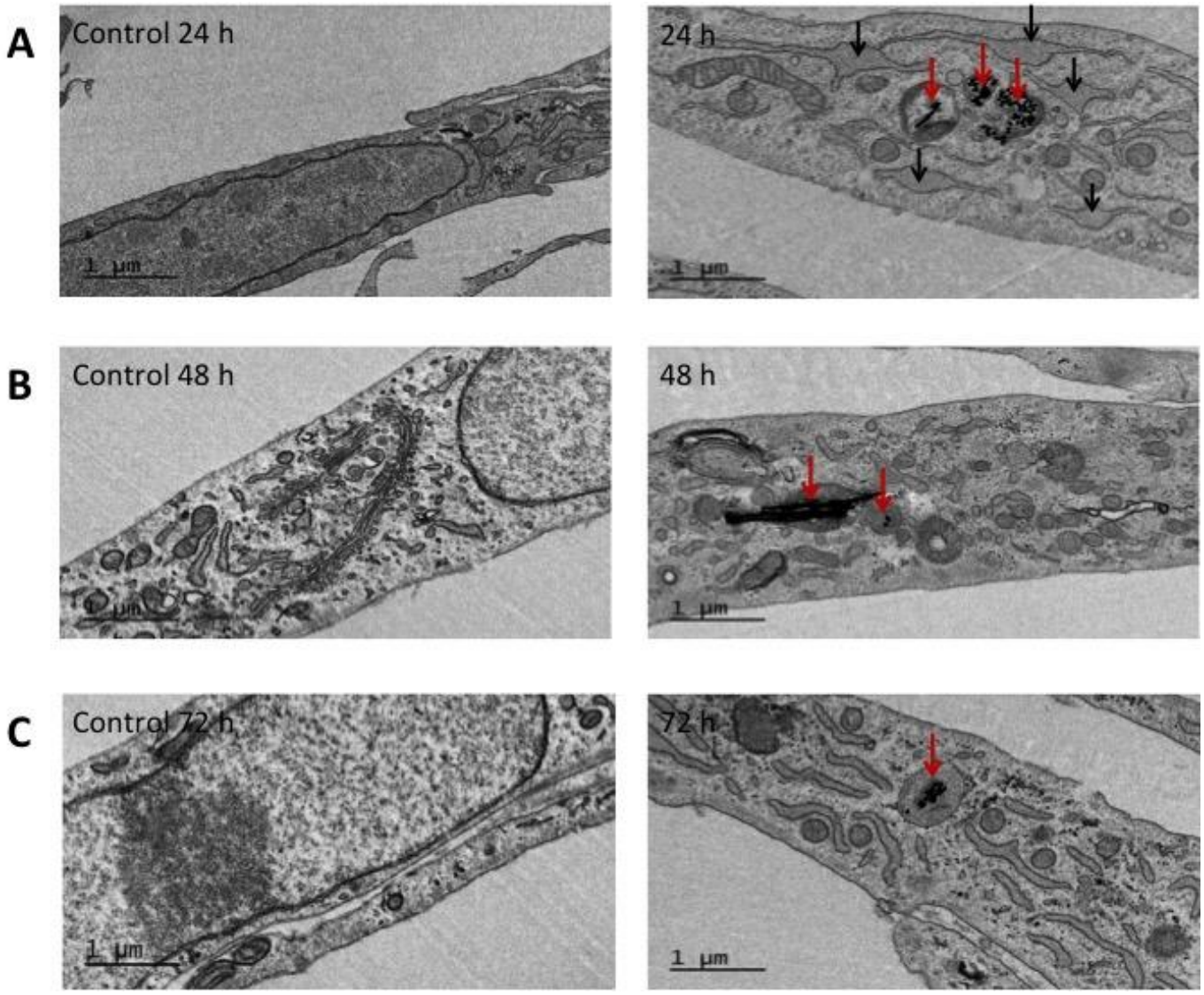

Figure 5. TEM images of Ni NWs aggregates. (A and B) The images show a subsection of human fibroblasts where Ni NWs are internalized or outside the cell and presented mainly random shape agglomerate.